Heterogeneous Pair Approximation of Methanol Oxidation on TiO_2 Reveals Two Reaction Pathways

Changhae Andrew Kim and Troy Van Voorhis*

Department of Chemistry, Massachusetts Institute of Technology, Cambridge, Massachusetts 02139, United States

E-mail: tvan@mit.edu

Abstract

We propose a novel method to simulate the chemical kinetics of methanol oxidation on the rutile TiO_2(110) surface. This method must be able to capture the effects of static disorder (site-to-site variations in the rate constants), as well as dynamic correlation (interdependent probabilities of finding reactants and products next to each other). Combining the intuitions of the mean-field steady state (MFSS) method and the pair approximation (PA), we consider representative pairs of sites in a self-consistent bath of the average pairwise correlation. Pre-averaging over the static disorder in one site of each pair makes this half heterogeneous pair approximation (HHPA) efficient enough to simulate systems of several species and calibrate rate constants. According to the simulated kinetics, a static disorder in the hole transfer steps suffices to reproduce the stretched exponentials in the observed kinetics. The identity of the dominant hole scavenger is found to be temperature-dependent – the methoxy anion at 80 K and the methanol molecule at 180 K. Moreover, two distinct groups of 5-coordinate titanium (Ti_{5c}) sites emerge – a high-activity group and a low-activity group – even though no

such division exists in the rate constants. Since the division is quite insensitive to the type of static disorder, the emergence of the two groups might play a significant role in a variety of photocatalytic processes on TiO_2.

Introduction

Methanol reforming is a chemical reaction that converts methanol and water into carbon dioxide and hydrogen gas, which has promising applications in fuel cells.[1–4] The reaction can be photocatalyzed on a TiO_2 surface,[5–7] where the first step is the oxidation of methanol to formaldehyde.[6] Both a practical reaction and a model system to emulate the decomposition of organic pollutants, the photocatalytic dissociation of methanol on the rutile $TiO_2(110)$ surface has been a subject of extensive research in both experimental[8–11] and theoretical[12–15] studies. Nonetheless, certain aspects of the reaction mechanism remain enigmatic.

While it has been established that photogenerated holes play a central role in methanol oxidation,[16–18] the identity of the hole scavenger continues to be debated. Based on density functional theory (DFT) and Bader charge analysis, it has been proposed that the cleavage of the OH bond is thermally activated, and the methoxy anion traps a hole to break the CH bond.[12,14] Meanwhile, Migani and Blancafort used spin-polarized DFT to show that an exciton can be localized in the TiO_2 lattice underneath a methanol molecule.[13] The hole can migrate up to the methanol molecule in a proton-coupled electron transfer (PCET), whence the methoxy radical can either reduce to a methoxy anion or proceed to a formaldehyde radical anion. However, the precise role of photogenerated holes in the cleavage of the OH bond continues to be questioned.[15]

Another mystery, the fraction of undissociated methanol decays as a stretched exponential of the irradiation time,[8–10,19] which is a signature of fractal kinetics.[20] Fractal kinetics is a term that encompasses a wide range of pathological behaviors that arise in heterogeneous systems, which might be intrinsic to the reaction mechanism or due to the geometry of the interface.[21] Indeed, a couple of explanations have been proposed on the origin

of the stretched exponentials.[9,10,19] On the one hand, methanol oxidation involves multiple, reversible steps.[9,12,22] A reaction network can give rise to an overall kinetics that is non-exponential. On the other hand, charge transport on the rutile $TiO_2(110)$ surface is disordered.[23,24] As the reactants on the most active sites are consumed, the effective rate coefficient might diminish over time. Wang et al. have measured the kinetics of methanol oxidation at multiple surface coverages and temperatures,[10] but there is not a mathematical and mechanistic model that helps to support either of the explanations.

Indeed, we are not aware of attempts to answer these questions via microkinetic modelling. This could be attributed to a couple of challenges. The first challenge is static disorder. For practical applications, the relevant surface is not the stoichiometric TiO_2, but the reduced TiO_{2-x}.[25] The non-stoichiometry entails surface and sub-surface oxygen vacancies, which affect the electronic structure in their vicinity and the chemistry at the surface.[26–28] There would be site-to-site variations in the rate constants, and using a single-valued rate constant per elementary step might not be sufficient to describe the disorderd kinetics. The second challenge is dynamic correlation. On the one hand, STM images show that the products of methanol oxidation tend to remain next to each other.[8,10,22] The uncorrelated products of probabilities, $[CH_3O^-][H]$ and $[CH_2O][H]$, are going to underestimate the rate of the reverse reaction. On the other hand, the diffusion of the formaldehyde at temperatures $\gtrsim 215\,\mathrm{K}$ inhibit the reverse reaction.[22,29] Hence, the relative positions of the reactants and the products should be taken into account.

In this paper, we propose a novel method to simulate the chemical kinetics of methanol oxidation on TiO_2. Combining the intuitions of the mean-field steady state (MFSS) method[30,31] and the pair approximation (PA),[32–35] we take representative pairs of sites and place them in a self-consistent bath of the average pairwise correlation. Then, we pre-average over the static disorder in one site of each pair, which gives a considerable reduction in the computational costs. This half heterogeneous pair approximation (HHPA) is efficient enough to simulate systems of several species and calibrate rate constants. We demonstrate these

capabilities using the experimental data of Wang et al.[10]

Comparison of mechanistic models point to an alternative route to thermal activation that can break the OH bond. In fact, the dominant hole scavengers are found to be temperature-dependent – the methoxy anion at 80 K and the methanol molecule at 180 K. The simulated kinetics appear to be insensitive to the details of charge transport inside the TiO_2 lattice, and a static disorder in the hole transfer to the methanol molecule and the methoxy anion suffices to reproduce the stretched exponentials in the observed kinetics. Remarkably, the static disorder gives rise to bimodal distributions in the coverages and the rates, even though the rate constants have a unimodal distribution. This implies that two groups of 5-coordinate titanium (Ti_{5c}) sites emerge with innate and disparate activities. Hence, there are not only two pathways that are active at different temperatures, but also two groups of Ti_{5c} sites that have different activities. Since the division appears to be quite insensitive to the type of static disorder, the emergence of the two groups might play a significant role in a variety of photocatalytic processes.

Theory

Mathematical Models

A sure way to capture the effects of static disorder and dynamic correlation is kinetic Monte Carlo (KMC).[36–38] However, the size of the lattice and the number of trajectories that are required to converge the stochastic simulation often make it impractical to use KMC to calibrate rate constants. Besides, the desired outcomes of chemical kinetics simulations are often ensemble average quantities, such as surface coverages and reaction rates. Therefore, it makes sense to write the kinetic equations in the occupation probabilities of n-site clusters (n-site probabilities).

The kinetic equations of one-site clusters are

$$\begin{aligned}\frac{d[X_i]}{dt} = &+ \sum_A k_{A_i \to X_i}[A_i] + \sum_{YAB} \sum_j k_{A_iB_j \to X_iY_j}[A_iB_j] \\ &- \sum_A k_{X_i \to A_i}[X_i] - \sum_{YAB} \sum_j k_{X_iY_j \to A_iB_j}[X_iY_j] \end{aligned} \tag{1}$$

where X_i denotes species X at site i; j runs over the nearest neighbors of site i; and $k_{A_iB_j \to X_iY_j}$ is the rate constant of the elementary step, $A + B \to X + Y$, with species A at site i and species B at site j, or zero if such step does not exist. For example, the first term describes the unimolecular reaction of the A to produce a X at its position, and the last term describes the bimolecular reaction of the X and a neighboring Y to produce a A and a B at their respective positions. On a uniform surface, the sites would have the same rate constants and occupation probabilities, so the indices could be dropped. On a non-uniform surface, the indices are required to capture the effects of static disorder.

Notice that the equations are not closed, since two-site probabilities are required to describe bimolecular reactions. In general, the kinetic equations of n-site clusters depend on the $(n+1)$-site clusters. These n-site probabilities are special cases of moments, and we need a moment closure to approximate the higer-order moments using what we know about the lower-order moments. The simplest approximation is the mean-field (MF) approximation, $[X_iY_j] \approx [X_i][Y_j]$, which treats the occupation of neighboring sites as independent, or uncorrelated.

To capture the effects of correlation, we need the kinetic equations of at least two-site clusters

$$\begin{aligned}\frac{d[X_iY_j]}{dt} = &+ \sum_{BC} k_{B_iC_j \to X_iY_j}[B_iC_j] + \sum_{WAB} \sum_l k_{A_lB_i \to W_lX_i}[A_lB_iY_j] + \sum_{CDZ} \sum_m k_{C_jD_m \to Y_jZ_m}[X_iC_jD_m] \\ &- \sum_{BC} k_{X_iY_j \to B_iC_j}[X_iY_j] + \sum_{WAB} \sum_l k_{W_lX_i \to A_lB_i}[W_lX_iY_j] + \sum_{CDZ} \sum_m k_{Y_jZ_m \to C_jD_m}[X_iY_jZ_m] \end{aligned} \tag{2}$$

where l runs over the nearest neighbors of i that are not j; and m runs over the nearest neighbors of j that are not i. For example, the first term describes the reaction of the BC pair to produce a XY pair at its position, and the last term describes the reaction of the Y in the XY pair and a neighboring Z to produce a C (making a XC pair) and a D at their respective positions. We have treated unimolecular reactions as special cases of bimolecular reactions where one of the reactants is a spectator.

Now, we need to approximate the three-site probabilities in terms of the two-site probabilities. Using the definition of conditional probability, we can write

$$[X_i Y_j Z_m] \approx \frac{[X_i Y_j][Y_j Z_m]}{[Y_j]} \tag{3}$$

Known as the pair approximation (PA), this formula has been invented by independent workers in chemistry,[32] population biology,[33,34] and epidemiology.[35] Some readers might be more familiar with stochastic closures, such as the normal,[39] Poisson,[40] and log-normal[41,42] closures. However, stochastic closures are derived using physical and mathematical arguments that are more relevant to homogeneous systems (solutions and colloids), where the moments are expected numbers of molecules $\in \mathbb{R}$, as opposed to heterogeneous systems (surfaces and interfaces), where the moments are occupation probabilities of sites $\in [0, 1]$. Moreover, stochastic closures are prone to instabilities and unphysical values even in their native systems.[43] PA is robust once we assign an appropriate value to the removable discontinuity at zero. Thus, we do not consider stochastic closures any further.

Next, we turn our attention to static disorder. Equations (1) and (2) make explicit treatment of the static disorder in the neighboring sites, so a large number of sites might need to be sampled to converge the average over the static disorder. It would be useful to replace the neighboring sites with a bath that reflects the average environment. Then, only a small number of representative sites would need to be treated in an explicit manner, and a weighted average over these sites could be used to update the bath in a self-consistent

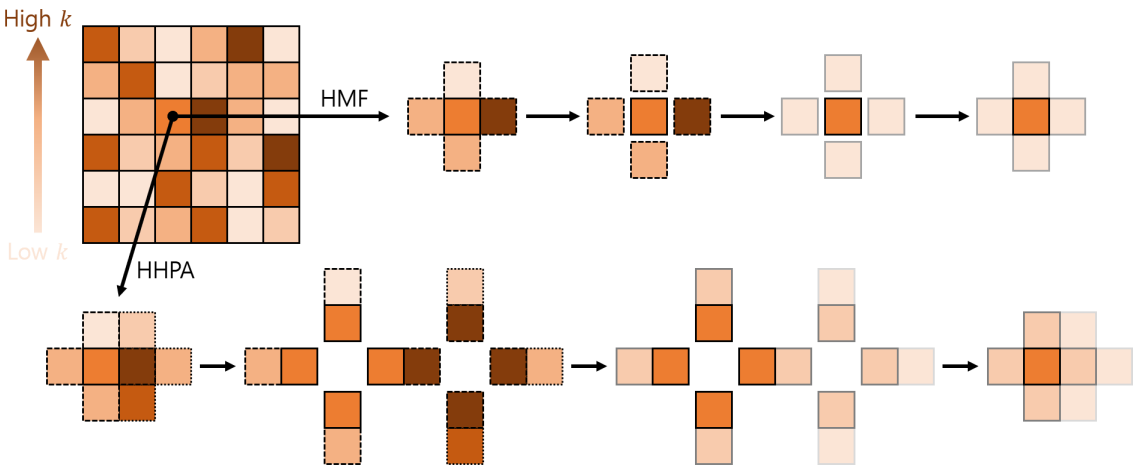

Figure 1: Graphical representations of HMF and HHPA.

manner. In other words, we want to replace

$$[B_j] \to \langle [B] \rangle = \frac{1}{M} \sum_{i=1}^{M} [B_i] = \int_k [B(k)] \rho(k) dk \approx \sum_k w_k [B_k] \tag{4}$$

where M is the number of sites on the lattice; $\rho(k)$ is the distribution of the rate constants; and w_k is a discretization of $\rho(k)dk$. Thus, we transform a sum over the sites of the lattice to an integral over the rate constants, which can be approximated as a weighted sum over some representative sites.

To simplify the transformation, we need a few assumptions. First, we assume that the static disorder can be represented as a one-dimensional distribution. If the effects of the static disorder are embodied in the height of a barrier, then the rates of the forward and the reverse reactions that cross this barrier are going to be modulated together. If the effects of the static disorder are embodied in the stability of a reactant, then the rate constants of the reactions that consume this reactant are going to be modulated together. Second, we assume that the static disorder is site-by-site. For unimolecular reactions, this means that the rate constants at sites i and j are independent. For bimolecular reactions, we assume that one of the reactants or the products dictates the reactivity, so the site that starts with the the reactant or ends with the product determines the rate constant. Hence, we write

$k_{A_iB_j\to X_iX_j} \to k_{A_iB\to X_iY}$ or $k_{B_jA\to Y_jX}$.

Figure 1 gives graphical representations of the heterogeneous mean-field (HMF) approximation and the half heterogeneous pair approximation (HHPA). The HMF equations are

$$\begin{aligned}\frac{d[X_i]}{dt} = &+ \sum_A k_{A_i\to X_i}[A_i] + \sum_{YAB} N_{XY} k_{A_iB\to X_iY}[A_i]\langle[B]\rangle + \sum_{YAB} N_{XY}\langle k_{BA\to YX}[B]\rangle[A_i] \\ &- \sum_A k_{X_i\to A_i}[X_i] - \sum_{YAB} N_{XY} k_{X_iY\to A_iB}[X_i]\langle[Y]\rangle - \sum_{YAB} N_{XY}\langle k_{YX\to BA}[Y]\rangle[X_i] \quad (5)\end{aligned}$$

where N_{XY} is the number of nearest neighbors. The subscripts in N_{XY} are required to accomodate the anisotropy of the lattice, if any. In essence, we have taken the neighbors of the main site and replaced them with the ensemble average site. The mean-field steady state (MFSS) method can be obtained by setting the left hand side of the HMF equations to zero and solving to obtain the steady state probabilities.[30,31]

Notice that terms of the form, $\langle k_{BA\to YX}[B]\rangle$, appear in the equations. These are not the same as $\langle k_{BA\to YX}\rangle\langle[B]\rangle$. The average of the product combines the effects of the static disorder on the rate constants and the effects of the rate constants on the occupation probabilities to give the effective rate. However, the product of the averages erases the dependence of the occupation probabilities on the rate constants.

As the MF part of its name indicates, HMF neglects the dynamic correlation of the main site with the neighboring sites. It replaces the neighboring sites with the ensemble average site that has no connection to the main site. Hence, not reflected in the rates are the unlikelihood of finding reactants next to each other and the likelihood of finding products next to each other due to the finite diffusivity of the adsorabates. To recover the effects of dynamic correlation, we need to write the kinetic equations in terms of higher-order clusters.

Naively, we might take the kinetic equation of two-site clusters and replace the neighboring site terms with conditional averages, such as

$$[A_lB_i] \to \langle[B_iA]\rangle = \sum_k w_k[B_iA_k] \quad (6)$$

which gives the probability of finding species B at site i along with species A at a generic neighboring site. Similar methods have been successful in epidemiology[44] and network theory.[45] Unfortunately, the same approach is unlikely to be useful in chemical kinetics. The presence of two indices i and j in the main pair means that the number of equations is quadratic. If M sites with distinct rate constants are required to describe the distribution of rate constants at the one-site level, then $M(M+1)/2$ pairs are required at the two-site level. For a system of S species, the full heterogeneous pair approximation would contain $S^2M(M+1)/2$ variables. This might not be a problem in systems of two to three species, such as the susceptible-infected-recovered (SIR) model[46] or the voter model.[47] However, chemists are often interested in systems containing multiple reactants, intermediates, and products.

To reduce the computational costs, we take advantage of the assumption that the static disorder is site-by-site. We pre-average over the static disorder in one of the main sites and change the variables, $[X_iY_j] \rightarrow [X_iY]$. Note that averaging over the static disorder does not amount to erasing the correlation. The variables, $[X_iY]$, are conditional averages in Equation 6, which consider the simultaneous occupation probabilities of site i and its generic neighbor. Hence, the effects of site i on its neighboring sites and vice versa are treated in an average sense. As a point of contrast, HMF reduces to uniform MF on a uniform surface, whereas HHPA reduces to uniform PA.

The HHPA equations are

$$\begin{aligned}
\frac{d[X_iY]}{dt} = &+ \sum_{BC} k_{B_iC\to X_iY}[B_iC] \\
&+ \sum_{BC} \frac{\langle k_{CB\to YX}[CB]\rangle}{\langle [CB]\rangle}[B_iC] \\
&+ \sum_{WAB} N_{WXY} k_{B_iA\to X_iW} \frac{[B_iA][B_iY]}{[B_i]} \\
&+ \sum_{WAB} N_{WXY} \frac{\langle k_{AB\to WX}[AB]\rangle}{\langle [AB]\rangle} \frac{[B_iA][B_iY]}{[B_i]} \\
&+ \sum_{CDZ} N_{XYZ} \left\langle k_{CD\to YZ} \frac{[CX][CD]}{[C]} \right\rangle \frac{[X_iC]}{\langle [CX]\rangle} \\
&+ \sum_{CDZ} N_{XYZ} \frac{\langle k_{DC\to ZY}[DC]\rangle}{\langle [DC]\rangle} \left\langle \frac{[CX][CD]}{[C]} \right\rangle \frac{[X_iC]}{\langle [CX]\rangle} \\
&- (ABCD \leftrightarrow WXYZ)
\end{aligned} \tag{7}$$

where N_{WXY} and N_{XYZ} are the numbers of nearest neighbors that are not one of the main sites; and the notation $(ABCD \leftrightarrow WXYZ)$ replicates the previous terms with the roles of the reactants and products exchanged. Namely, we have written down terms that produce an X_iY pair and gathered terms that consume an X_iY pair in $(ABCD \leftrightarrow WXYZ)$. In the first and third terms, the reactions are centered on site i, so the rates are described using the explicit rate constants, such as $k_{B_iC\to X_iY}$. In the second and fourth terms, the reactions involve site i but are centered on the neighboring site, so the rates are described using the effective rate coefficients, such as $\langle k_{AB\to WX}[AB]\rangle/\langle [AB]\rangle$. The fifth and sixth terms are formulated to preserve the equality, $\langle [XY]\rangle = \langle [YX]\rangle$, provided that the initial conditions satisfy it.

The assumption that the static disorder is site-by-site might break down in systems where point defects are not the dominant type of defects, or if the rate of reaction has intrinsic dependence on multiple sites. Even in systems where the site-by-site assumption holds, the pre-averaged neighbor might not be sufficient to capture the effect of the neighboring sites

on site i, if pairs with extreme values of rate constants on both sites have an important role on the kinetics. However, the same weaknesses also affect HMF. In Section S1, we compare the performances of HMF and HHPA on a number of simple model systems, and HHPA gives qualitative improvements over HMF in every case. Although PA is not satisfactory in systems with significant long-range correlation, it can exhibit semi-quantitative accuracy in systems with only short-range correlation. Therefore, we expect HHPA to give a reasonable description of methanol oxidation on TiO_2.

We have implemented the above methods in a C code that computes the rates and the Jacobian of a user-input reaction mechanism using a choice of uniform MF, uniform PA, HMF, and HHPA. The code is available on GitHub (`https://github.com/changhae-kim/hmca`).

Mechanistic Model

For the purposes of simulating methanol oxidation, the rutile $TiO_2(110)$ surface can be regarded as a rectangular lattice with alternating rows of 5-coordinate titanium sites (Ti_{5c}) and bridging oxygen sites (O_b).[25,48] The non-stoichiometry of the reduced TiO_{2-x} implies that 9 % to 10 % of the O_b sites are replaced with bridging oxygen vacancies (O_v).[10] Methanol can adsorb on one of the two positions: the Ti_{5c} sites, where molecular adsorption is favored; and the O_v sites, where dissociative adsorption is favored.[49–52] The active sites in the photocatalytic dissociation of methanol appear to be the Ti_{5c} sites,[8,9] and Wang et al. only counted the adsorbates on the Ti_{5c} sites.[10] Therefore, we do not consider O_v sites in our model.

Figure 2 illustrates a mechanistic model of methanol oxidation. The model includes most reactions that have been proposed to take place during the irradiation of methanol on TiO_2, along with their reverse reactions.[11–14,29] Only, we do not consider the cross-coupling of methanol and formaldehyde, which has been shown to be negligible at coverages $\lesssim 0.15$ monolayer (ML).[53]

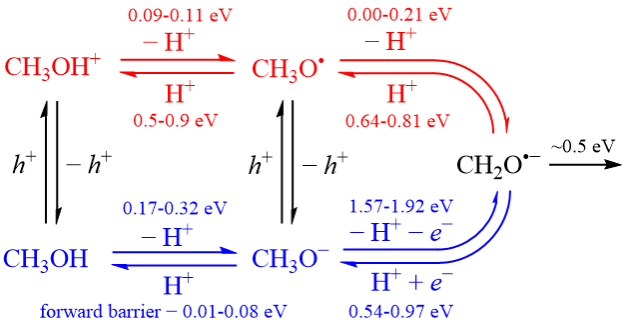

Figure 2: Mechanistic model of methanol oxidation on TiO_2. The expected values of the activation energies are based on a number of DFT studies.[11–14,29]

Along the bottom of Figure 2, the steps in blue represent the cleavage of the OH bond and the CH bond in the methanol molecule and the methoxy anion, respectively. Notice that the reactions do not involve photogenerated holes. For these *thermally activated* steps, a multitude of DFT studies have established the expected values of the activation energies. The OH bond cleavage is endothermic by 0.01 eV to 0.08 eV, and both the forward and the reverse reactions should be accessible, with the forward barrier of 0.17 eV to 0.32 eV.[12–14] On the other hand, the CH bond cleavage is much more endothermic, and only the reverse reaction might be accessible, with the barrier of 0.54 eV to 0.97 eV.[12,14]

Along the top of Figure 2, the steps in red represent the cleavage of the OH bond and the CH bond in the methanol "cation" and the methoxy radical, respectively. Notice that the reactants have trapped a hole in some capacity. For these *hole-activated* steps, the feasibilities and the activation energies are debated. Indeed, it is uncertain whether the methanol molecule would trap a hole. Given the mechanistic resolution of chemical kinetics, our model does not distinguish between a hole trapping at the methanol molecule and a hole trapping at a nearby position in the TiO_2 lattice. The reactant CH_3OH^+ might not be a methanol cation per se, but a methanol molecule with an exciton or a hole in the TiO_2 lattice underneath. According to computational studies that managed to place an exciton[13] or a hole[11] underneath the methanol molecule, the OH bond cleavage becomes exothermic, and the forward barrier reduces to 0.09 eV to 0.11 eV. Meanwhile, there is no dispute that the methoxy anion would trap a hole. Studies have found that the CH bond cleavage should

be almost barrierless,[11,13] or it might have a modest activation energy of 0.21 eV.[14]

The reactants of the thermally activated steps and the hole-activated steps can interchange via charge transfer, which are the vertical steps in Figure 2. Finally, the formaldehyde can diffuse along the Ti_{5c} rows with the activation energy ~ 0.5 eV,[29] which prevents the recomposition of methanol.[22]

According to the mehcanistic model, the methanol molecule has a number of routes to the formaldehyde radical anion. Since the cleavage of the CH bond in the methanol anion should be inaccessible,[12] we can dismiss the the themally activated pathway: $CH_3OH \rightarrow CH_3O^- \rightarrow CH_2O^{\cdot -}$. Bader charge analysis indicated that the methanol molecule is unlikely to trap a hole.[14,15] Shen and Henderson irradiated surfaces covered in methanol and methoxy, respectively, and found that the photocatalytic dissociation of methoxy is an order of magnitude faster than that of methanol at 100 K to 120 K.[54] These results have motivated a pathway where the cleavage of the OH bond is thermally activated and then the methoxy anion traps a hole to break the CH bond: $CH_3OH \rightarrow CH_3O^- \rightarrow CH_3O^{\cdot} \rightarrow CH_2O^{\cdot -}$.[12,14] Meanwhile, Migani and Blancafort found that an exciton can be localized in the TiO_2 lattice underneath a methanol molecule.[13] Hou et al. found using scanning tunneling microscopy (STM) that the direct injection of a hole into the TiO_2 surface can initiate one-step conversions of methanol to methoxy, methoxy to formaldehyde, and methanol to formaldehyde.[11] These results have motivated an alternative pathway where the hole mediates the cleavage of the OH bond and the CH bond: $CH_3OH \rightarrow CH_3OH^+ \rightarrow CH_3O^{\cdot} \rightarrow CH_2O^{\cdot -}$.[11,13] However, Ma et al. have proposed that the holes might only contribute vibrational energy in the cleavage of the OH bond.[15]

In our model, the presence of CH_3OH^+ provides an alternative route to thermal activation, where the cleavage of the OH bond proceeds with a different set of rate constants. This can be justified as follows. Even if the hole did not become trapped at the methanol molecule per se, if the hole were close enough to transfer its energy, then the subsequent transfer of the hole itself could be instantaneous. Unlike the thermally activated route, the

hole-mediated cleavage of the OH bond is not reversible until a charge transfer has taken place. Since the OH bond cleavage is expected to be fast in either case, we might not be able to discern whether the hole changes the barrier or only contributes the vibrational energy to overcome the original barrier. Nonetheless, we should be able to determine the kinetic relevance of photogenerated holes in the cleavage of the OH bond.

Model Parameters

Wang et al. measured the kinetics of methanol oxidation at a number of surface coverages between 0.01 ML and 0.11 ML and at the temperatures of 80 K and 180 K.[10] To calibrate the relevant parameters, we minimize the root mean square normalized error (RMSNE) of the simulated kinetics. Namely, the error at each point is normalized to the uncertainty of the experimental data, which is a common practice in regression.

We assume that the rate constants of the molecular steps obey the transition state theory

$$k_r(T) = Q_r \frac{k_\mathrm{B}T}{h} e^{-\Delta E_r^\ddagger / k_\mathrm{B}T} \tag{8}$$

where $\Delta E_r^\ddagger$ is the activation energy and Q_r is the partition function. The expected values of the activation energies are summarized in Figure 2. In principle, the partition functions are temperature-dependent. However, we assume that they are almost constant and require that their values are 10^{-2} to 10^2.

Meanwhile, we assume that the charge carrier dynamics take place at a faster timescale than the molecular dynamics. This implies that the charge transfer steps can be approximated as unimolecular reactions of the methanol and the methoxy adsorbates, with an effective rate constant, $k_r = k_r'[h^+]$. Since these effective rate constants combine the effects of the charge carrier density and mobility, they might not have a simple dependence on temperature. The mobility of the charge carriers increases as the temperature increases, which in turn increases their recombination.[55] Hence, we treat the effective rate constants of charge

transfer at the two temperature as independent parameters.

To describe the effects of static disorder, we apply a Boltzmann factor to the effective rate constants of hole transfer to the methanol molecule and the methoxy anion

$$k_r^i(T) = k_r^0(T) e^{-\Delta E_i / k_\mathrm{B} T} \tag{9}$$

where ΔE_i represents the site-to-site variation in the trap energies. Indeed, we conjecture that the disparate abilities of sites to transfer a hole to the adsorbates arises due to hole trapping and detrapping. Given the 3.03 eV band gap of the rutile TiO_2,[56,57] it is dubious whether the deep trap states in the middle of the band gap can participate in the photochemistry, so we focus on the shallow trap states that contribute to the band gap narrowing. Thus, we expect that ΔE_i would have a Poisson distribution, associated with the Urbach tail at the band edge of a disorderd semiconductor[58]

$$\rho(\Delta E) \propto e^{-\Delta E / E_\mathrm{U}}, \Delta E > 0 \tag{10}$$

where E_U is the Urbach energy that controls the amount of static disorder. Since the static disorder affects the trap energies on the TiO_2 side only, we do not apply the Boltzmann factor in the back transfer of the hole to the lattice.

Overall, the mechanistic model has 27 parameters: 4 charge transfer rate constants at 80 K; 4 charge transfer rate constants at 180 K; 9 activation energies; 9 partition functions; and the Urbach energy.

One of the most undesirable outcomes in regression is overfitting. If a model is given too many degrees of freedom, then it starts fitting to irrelevant information, such as the noise in the experimental data. In a mechanistic model, the parameters have an intuitive interpretation due to the topology of the model, so overfitting would yield values that are inconsistent with the interpretation. Fortunately, our goal is not to find unknown values in the dark. Our model has an extensive collection of expected values, so it should not be

difficult to detect signs of overfitting. It would give substantial confidence in the mechanistic model if a fit could be obtained with the parameters in reasonable ranges.

Results and Discussion

Simulated Kinetics

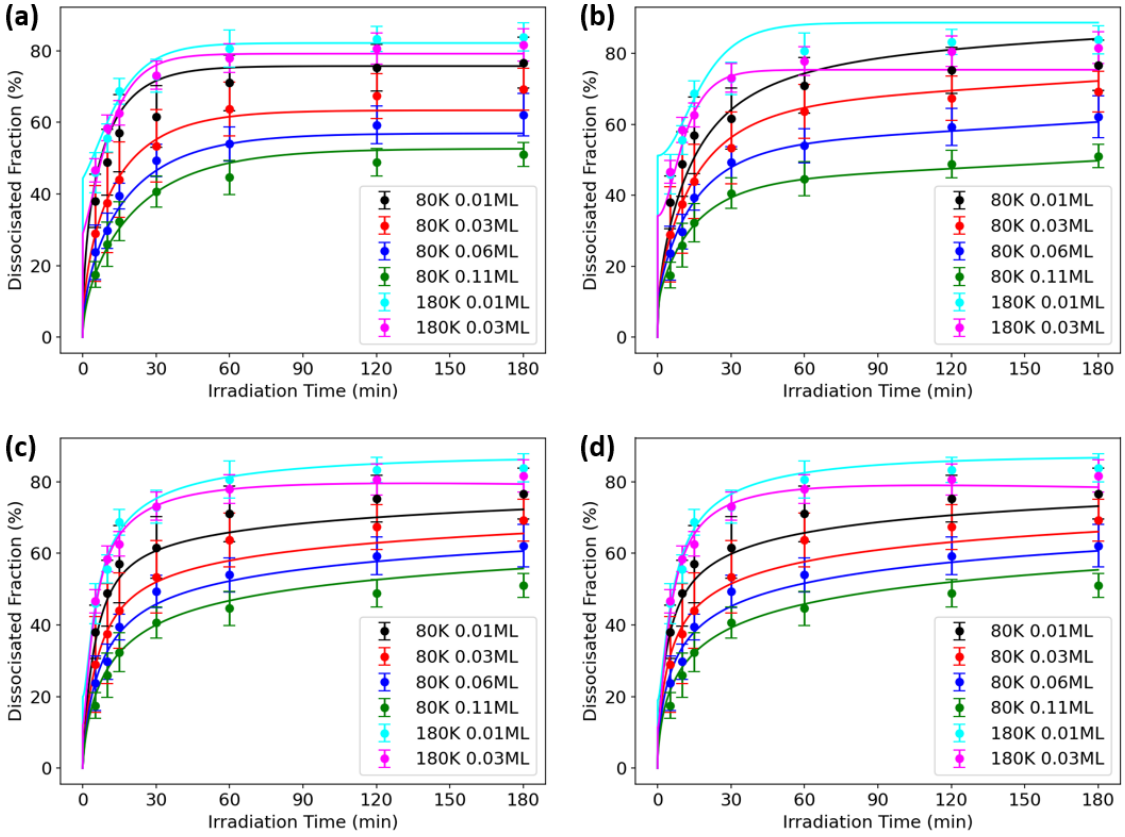

Figure 3: Time-dependent dissociated fractions in (a) uniform MF, RMSNE = 0.781; (b) uniform PA, RMSNE = 0.795; (c) HMF, RMSNE = 0.542; and (d) HHPA, RMSNE = 0.589.

Figures 3a and 3b show the simulated kinetics in uniform MF and PA, respectively. RMSNEs are 0.781 in MF and 0.795 in PA, which means that the simulated kinetics tend to be within a standard deviation of the experimental kinetics. However, a visual inspection reveals a number of issues. In the short time, the simulated kinetics in MF and PA both exhibit a transient at 180 K, where the dissociation fraction jumps, switches to a concave

growth, and then switches back to a convex growth. There is no evidence of such behavior in the STM images or the time-dependent two-photon photoemission (2PPE) spectra.[8,9,19] In the long time, the simulated kinetics in MF reach a steady state, and the simulated kinetics in PA also reach a steady state at 180 K. Again, these are inconsistent with the observed kinetics, which slow down but do not reach a steady state in hours of measurement.[8,9,19]

Figures 3c and 3d are the simulated kinetics in HMF and HHPA, respectively. RMSNEs have decreased to 0.542 in HMF and 0.589 in HHPA, and the simulated kinetics are now in good agreement with the experimental kinetics. In the short time, the transient at 180 K is suppressed to a point that it is inconspicuous. In the long time, the simulated kinetics slow down but do not reach a steady state in the simulation time, as desired. The improvements can be rationalized as follows. Due to the static disorder, there are sites with disparate rates of hole transfer. As the reactants on the most active sites are consumed, more and more inactive sites come to dominate the kinetics. Hence, the simulated kinetics in HMF and HHPA behave like a sum of multiple kinetics. On the one hand, there are the fast components that exhibit a rapid growth in the short time, so the transient must be suppressed to avoid overshooting the experimental kinetics. On the other hand, there are the slow components that make up the tail in the long time.

Even though the MF methods attain RMSNEs that are somewhat smaller than the PA methods, we emphasize that MF is not as faithful to the physical reality as the PA, since the products of methanol oxidation tend to remain next to each other. To demonstrate that MF and PA simulate somewhat different realities, we entered the parameters that were calibrated using the MF methods into the PA methods and vice versa. In short, entering the MF parameters into PA stretches the dynamics to the right, and entering the PA parameters into MF shrinks the dynamics to the left. The details can be found in Section S2.

Comparing the simulated kinetics in the uniform and the heterogeneous methods, we propose that static disorder might be required to reproduce the observed kinetics. As discussed in Introduction, there have been a couple of explanations on the origin of the stretched ex-

ponentials in the observed kinetics. One explanation was that multiple, reversible steps give rise to an overall kinetics that is non-exponential, and the other explanation was that static disorder in the rate constants gives rise to an effective rate coefficient that diminishes over time. While it is true that the uniform methods predict non-exponential kinetics, they do not resemble the stretched exponentials in the observed kinetics.[8,9,19] In particular, the short time behavior at 180 K contains a transient that is not observed in experiments. Meanwhile, assuming a simple distribution of trap energies is sufficient to give a good fit to the experimental kinetics and a suppression of the transient. Thus, the simulations seem to suggest that the static disorder in the hole transfer gives rise to the stretched exponentials.

It is also noteworthy that the simulated kinetics appear to be insensitive to the details of charge transport inside the TiO_2 lattice. As discussed in Methods, we have assumed that the charge carrier dynamics take place at a faster timescale than the molecular dynamics and treated the charge transfer steps as unimolecular reactions of the methanol and the methoxy adsorbates with an effective rate constant. Thus, the simulations are oblivious to what the charge carriers are doing inside the TiO_2 lattice, except that the photogenerated holes favor certain sites over others. Furthermore, the static disorder in the charge transport is embodied in the Urbach energy, which is a shared parameter across different surface coverages and temperatures. Wang et al. have proposed that the differences in the observed kinetics at different surface coverages might be attributed to the adsorbates scattering the photogenerated holes.[10] We do not find evidence of such sophisticated interactions. Instead, the competitive inhibition due to the consumption of O_b sites appears to be sufficient to capture the coverage-dependence.

Since the role of photogenerated holes in the cleavage of the OH bond is controversial, we also considered a modified model where the methanol cation has been removed. We provide the details in Section S3 and discuss the key results here. Using the modified model, we are unable to obtain RMSNE < 1 in uniform MF or PA, and the short time behavior again contains the transient at 180 K. HMF and HHPA also find higher RMSNEs of 0.910 and

0.981, respectively. As shown in Figures S5c and S5d, the primary source of error appears to be the short time behavior at 180 K. The simulated kinetics at 180 K exhibit significant divergence at different surface coverages, whereas the experimental kinetics are almost on top of each other. Thus, including an alternative route to the OH bond cleavage entails a significant improvement in the simulated kinetics, and the hole-activated cleavage of the OH bond appears to play an important role in methanol oxidation.

Rates and Rate Constants

Figures 4a and 4b summarize the time-averaged coverages (occupation probabilities) and rates at 80 K and 180 K, respectively. Note that these are rates and not rate constants. Further note that the plus-minus values indicate the spreads in the coverages and the rates due to the static disorder, not uncertainties.

The fastest steps at both temperatures are the thermally activated cleavage and reformation of the OH bond. Since the interconversion is orders of magnitude faster than any of the other steps, it gives rise to a quasi-equilibrium between the methanol molecule and the methoxy anion. Of course, fast is relative, and the interconversion is slow enough at 80 K to allow the methanol and the methoxy adsorbates to appear as distinct species in STM images. Meanwhile, the interconversion is much faster than a second at 180 K. In fact, the transient in the simulated kinetics at 180 K might be attributed to the rapid equilibration.

The dominant pathways of the forward reaction involve a hole transfer to the methoxy anion at 80 K and the methanol molecule at 180 K. In each case, the rates of the subsequent steps are almost equal to the rate of the hole transfer, which implies that the forward reaction almost always goes to completion once the hole transfer takes place. Hence, the hole transfer to the methoxy anion at 80 K and the methanol molecule at 180 K are the rate-limiting steps at the respective temperatures. In particular, it follows that the methanol molecule is the dominant hole scavenger at 180 K. Even though the thermally activated cleavage of the OH bond is orders of magnitude faster, the methoxy anion tends to revert to the methanol

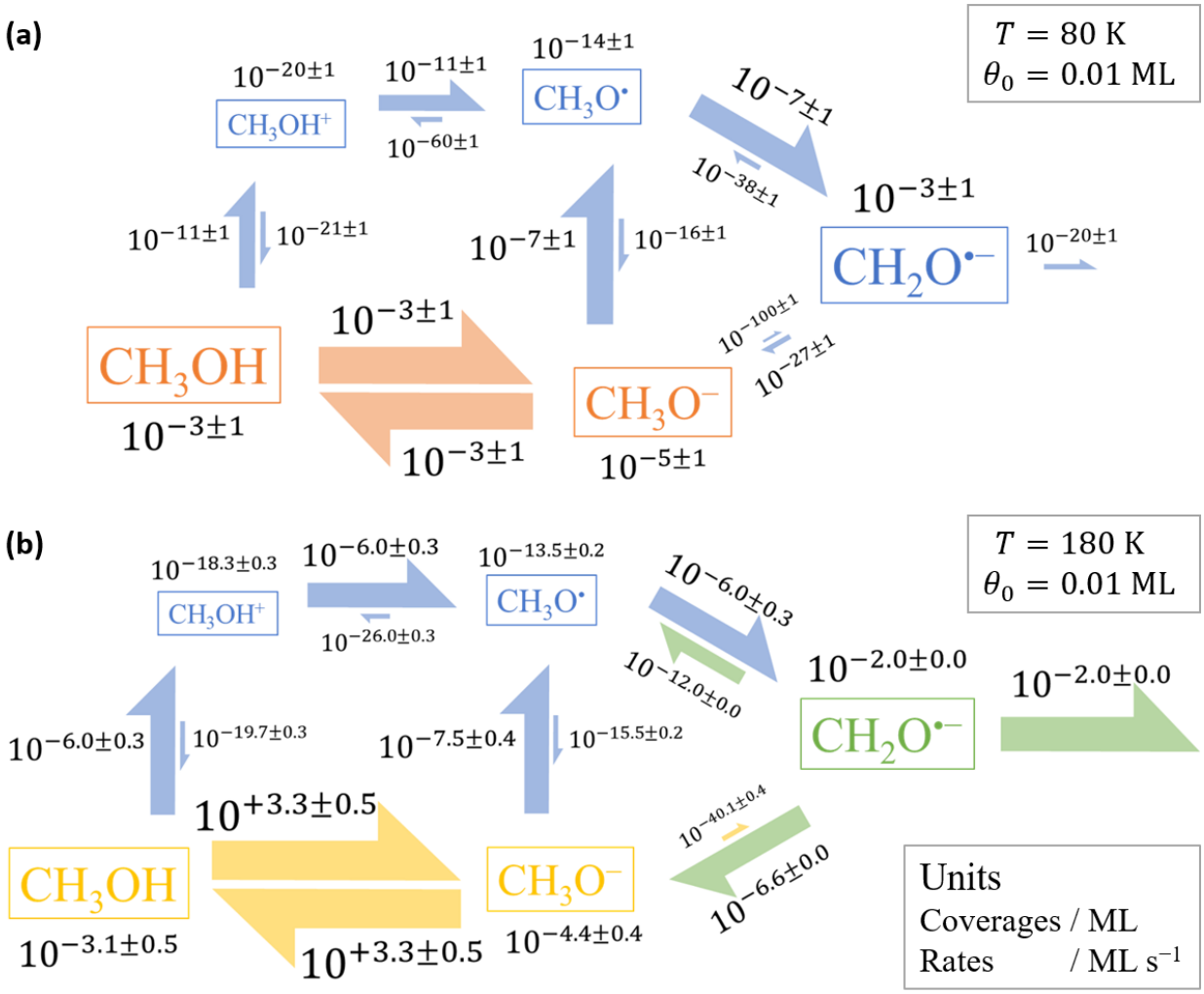

Figure 4: Time-averaged coverages and rates at (a) 80 K and (b) 180 K in HHPA. Roughly, the sizes of the boxes and the arrows relate to the magnitudes of the coverages and the rates, respectively. The units of the coverages and the rates are ML and ML s^{-1}, respectively. Note that the plus-minus values are the spreads in the coverages and the rates due to the static disorder, not uncertainties. The colors indicate different distributions of coverages and rates: blue indicates a unimodal distribution; and orange, yellow, and green indicate bimodal distributions with different weights. For the details, refer to Figure 5.

molecule before it traps a hole. It is the hole-activated cleavage of the OH bond that takes the reaction to completion and determines the overall kinetics. Note that these results are so far consisent with the experimental outcomes of Shen and Henderson,[54] since their experiments were conducted at 100 K to 120 K only. It is also worth noting that Shen and Henderson considered surfaces covered in only one of methanol and methoxy at a time, which gives a measure of rate constants and not rates. Accurate comparison of the outcomes would require taking the relative abundances of methanol and methoxy into account.

The dominant pathway of the reverse reaction is thermally activated at both temperatures. Since the methoxy anion is in quasi-equilibrium with the methanol molecule, the thermally activated reformation of the CH bond is the rate-limiting step. Meanwhile, the diffusion of the formaldehyde is significant at 180 K, and it appears to outcompete the reverse reaction.

To establish the upper and the lower bounds on the calibrated parameters, we performed sensitivity analysis by perturbing each of the parameters and recording the response of RMSNE. We provide the details in Section S4 and discuss the key results here. In the end, there are 9 parameters that have a well-defined optimum: the activation energies and the partition functions of the rate-limiting steps and the quasi-equilibrium steps, as well as the Urbach energy, which controls the amount of static disorder. The fast steps ensuing a rate-limiting step do not matter as long as the rate constants are greater than the rate-limiting step, and the slow steps competing with a rate-limiting step or a fast step do not matter as long as the rate constant is smaller than the relevant step. Thus, we can construct a compact model, where we set most of the rate constants to zero or a large value. Again, we provide the details in Section S5. The compact model gives RMSNEs on par with the original model, and the calibrated parameters tend to be within a narrow range of the parameter space, suggesting that the 9 parameters have an optimum not only when perturbed one at a time, but also in the multi-dimensional parameter space.

Interestingly, the effective rate constant of the hole transfer to the methoxy anion must

be at least an order of magnitude smaller at 180 K than it is at 80 K, as shown in Table S1. The non-Arrhenius behavior is not an artifact of the mechanistic model containing a back transfer step. As discussed above, the rate constants of the back transfer steps can be set to zero with no consequence on RMSNE, so the back transfer is not effective at counteracting the hole transfer. The non-Arrhenius behavior is also not an artifact of the mechanistic model containing the methanol cation. As shown in Table S2, the modified model with no hole transfer to the methanol molecule also predicts that the effective rate constant of the hole transfer to the methoxy anion is orders of magnitude smaller at 180 K than it is at 80 K. Hence, the non-Arrhenius behavior appears to be intrinsic to the physics of the hole transfer.

We can make sense of the non-Arrhenius behavior using the expression of the effective rate constant

$$k_r(T) \propto [h^+(T)]e^{-\Delta E_r/k_\mathrm{B}T} \tag{11}$$

where ΔE_r is the activation energy; and $[h^+(T)]$ is the quasi-steady state density of photo-generated holes at temperature T. As discussed in Theory, the charge carrier recombination increases as the temperature increases, so the hole density is a decreasing function of the temperature. While the Boltzmann factor is an increasing function of the temperature, it reduces to ≈ 1 if the activation energy is small enough. Indeed, computational studies have reported that it is easy to trap a hole at the methoxy adsorbate, and the hole transfer to the methoxy anion is downhill.[11,14] Then, the hole transfer might have a small barrier. It is plausible that the "effective" rate constant of the hole transfer to the methoxy anion can decrease as the temperature increases.

Furthermore, taking the ratios of the effective rate constants gives

$$\exp\left[(\Delta E_\mathrm{I} - \Delta E_\mathrm{II})\left(\frac{1}{k_\mathrm{B}T_1} - \frac{1}{k_\mathrm{B}T_2}\right)\right] = \frac{k_\mathrm{I}(T_1)/k_\mathrm{I}(T_2)}{k_\mathrm{II}(T_1)/k_\mathrm{II}(T_2)} \tag{12}$$

Substituting I = [$CH_3OH \rightarrow CH_3OH^+$], II = [$CH_3O^- \rightarrow CH_3O^\cdot$], $T_1 = 80\,\mathrm{K}$, and $T_2 = 180\,\mathrm{K}$, we deduce that $\Delta E_{CH_3OH\rightarrow CH_3OH^+} - \Delta E_{CH_3O^-\rightarrow CH_3O^\cdot} \gtrsim 0.2\,\mathrm{eV}$. Incidentally, this

value coincides with the *GW* results of Ma et al., which identified 3.91 eV and 3.70 eV as the excited states where the hole has a significant density on the methanol and the methoxy adsorbates, respectively.[15] While this is not sufficient evidence to conclude whether the methanol molecule can trap a hole, it is important to remember that chemical kinetics might not always proceed according to the energetics. Per molecule, the hole transfer to the methanol molecule is slower than the hole transfer to the methoxy anion at both temperatures. However, the relative abundance of the methanol molecule and the slowdown of the hole transfer to the methoxy anion appear to enable the methanol molecule to be the dominant hole scavenger at 180 K.

Distributions of Coverages and Rates

In the previous section, we noted spreads in the coverages (occupation probabilities) and the rates due to the static disorder. As discussed in Methods, only the effective rate constants of the hole transfer to the methanol molecule and the methoxy anion were assumed to differ site to site. Since the static disorder is contained in the hole transfer, the effects of the static disorder must be propagating throughout the reaction network. We have used colors to indicate the types of observed distributions in Figure 4.

Since the trap energies had a unimodal distribution, one might expect the coverages and the rates to exhibit a unimodal dsitribution, as well. Indeed, most of the coverages and the rates (blue in Figure 4) exhibit a unimodal distribution, as shown in Figure 5a. Remarkably, the coverages of the methanol molecule and the methoxy anion at 80 K (orange in Figure 4a) exhibit a bimodal distribution, as shown in Figure 5b. The sites with high and low coverages are divided into distinct groups, and the two groups appear to contain similar fractions of sites. Moreover, the sites with high and low coverages of the methanol molecule also have high and low coverages of the methoxy anion, respectively, as shown in Figure 5c. The correlation of the coverages might be attributed to the quasi-equilibrium of the methanol molecule and the methoxy anion.

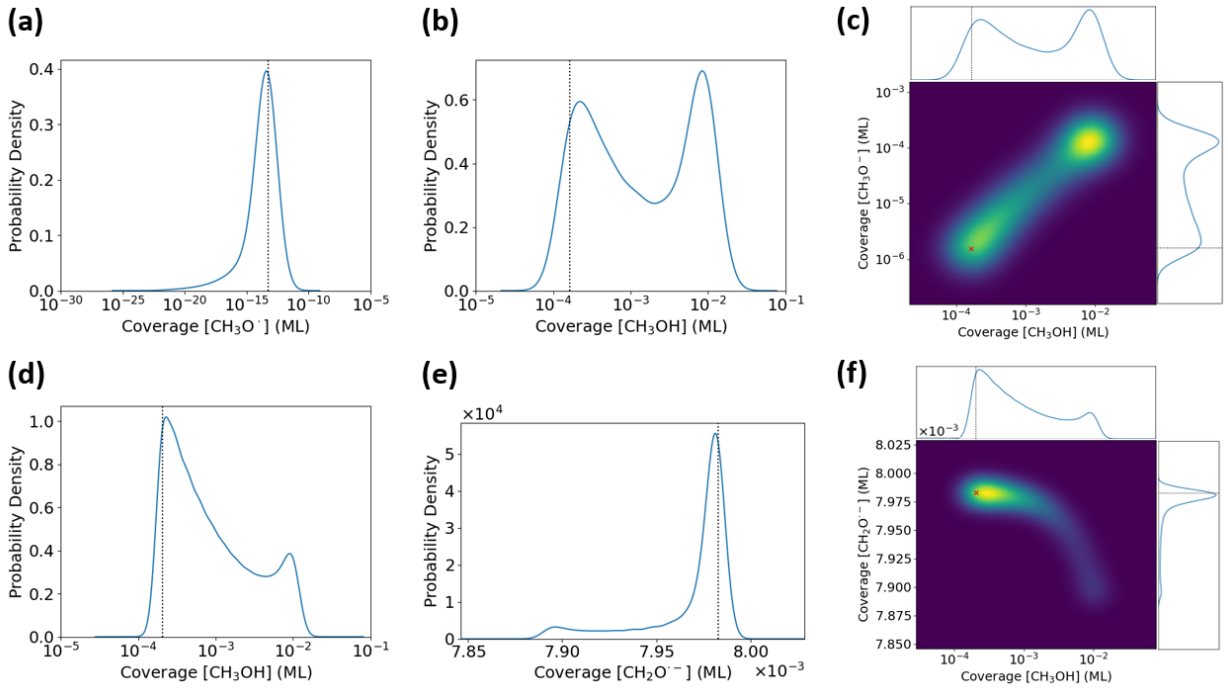

Figure 5: Time-averaged distributions of the coverages in HHPA: (a) the methoxy radical at 80 K, blue in Figure 4; (b) the methanol molecule at 80 K, orange in Figure 4a; (c) the methanol molecule and the methoxy anion at 80 K, both orange in Figure 4a; (d) the methanol molecule at 180 K, yellow in Figure 4b; (e) the formaldehyde at 180 K, green in Figure 4b; and (f) the methanol molecule and the formaldehyde at 180 K, yellow and green in Figure 4b, respectively. The dotted lines and the crosses mark the coverages of the site with $\Delta E_i = 0$, or $k_r^i = k_r^0$.

The coverages of the methanol molecule and the methoxy anion at 180 K (yellow in Figure 4b) continue to exhibit a bimodal distribution, as shown in 5d. Only, sites with low coverages are a majority, and sites with high coverages are a minority. The coverage of the formaldehyde at 180 K (green in Figure 4b) also exhibits a bimodal distribution, as shown in Figure 5e. For the formaldehyde, the weights are the opposite of the methanol molecule and the methoxy anion. Sites with high coverages of the formaldehyde are a majority, while the sites with low coverages of the formaldehyde make only a small bump on the distribution. Indeed, the sites with high and low coverages of the formaldehyde have low and high coverages of the methanol molecule, respectively, as shown in Figure 5f.

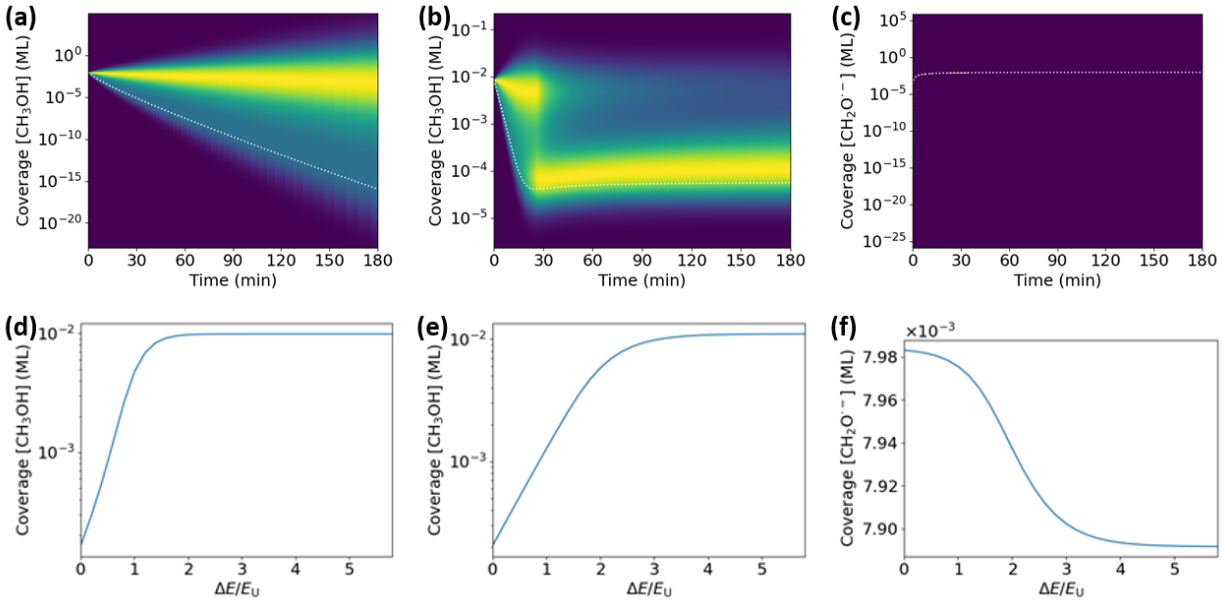

Figure 6: Time-dependent distributions of the coverages and coverages as a function of the trap energy: (a,d) the methanol molecule at 80 K; (b,e) the methanol molecule at 180 K; and (c,f) the formaldehyde at 180 K. The dotted curves mark the coverages of the site with $\Delta E_i = 0$, or $k_r^i = k_r^0$.

The bimodal distributions are not results of time-averaging, and they are manifest at each point in time. As shown in Figure 6a, the coverages of the methanol molecule and the methoxy anion at 80 K diverge in a monotonic manner. Meanwhile, the coverages of the two species at 180 K exhibit a peculiar behavior. As shown in Figure 6b, the group with high coverages is the majority in the short time. Then, there is an inversion at $t \approx$

25 min, whence the group with the low coverages takes the majority. Finally, the coverage in the formaldehyde at 180 K appears as a pixel-thin curve in Figure 6c. Even though the distribution resembles Figure 5e at each point in time, the spread is so narrow compared to the changes in the mean that it only undergoes translations on the most part. We provide a complete collection of the time-averaged and time-dependent distributions in Figures S19–S25. Furthermore, we note that the corresponding coverages and rates in the modified model and the compact model also exhibit bimodal distributions, as shown in Figures S26–S45.

Effectively, there are two groups of Ti_{5c} sites on the TiO_2 surface. On the high-activity sites, the hole transfer to the methanol molecule and the methoxy anion is rapid, so the reactants undergo rapid oxidation to the formaldehyde. On the low-activity sites, the hole transfer is slow, so the methanol molecule and the methoxy anion remain in quasi-equilibrium, with occasional oxidation to the formaldehyde. Hence, the high-activity sites end up with low coverages of the methanol molecule, and vice versa. The two groups of Ti_{5c} sites are not distinct in a discrete fashion, but they represent ranges on a continuum of trap energies. Thus, it makes sense that sites with low coverages of the methanol molecule increase at 180 K. At higher temperatures, higher barriers can be overcome, so more sites join the high-activity group. The surprising part is that there are few sites in the transition zone, and a continuous change in the rate constants appear to give an abrupt change in the rates, akin to a dynamical transition or a bifurcation in the reaction network.

Since a significant fraction of the sites have $\Delta E_i \sim k_B T$, it is not a surprise that a distinct high-activity group emerges. In Figure 5, we have marked the expected coverage of a site with $\Delta E_i = 0$, or $k_r^i = k_r^0$, and the mark coincides with the high-activity group, as expected. However, it is curious that a wide range of sites with $\Delta E_i \gg k_B T$ end up with similar coverages and give rise to the low-activity group. This is due to the limits on the coverages. As shown in Figures 6d and 6e, sites with only a few Urbach energies of trap energy are already so inactive that they retain the initial coverage of the methanol molecule. Meanwhile, the diffusion of formaldehyde at 180 K entails a minimum coverage even on these

inactive sites, as shown in Figure 6f. We expect that most types of static disorder with a long tail in the distribution of trap energies would lead to the emergence of the high-activity and the low-activity groups.

To establish the robustness of the division, we examined the normal, Poisson ($k = 2$), and hyperbolic secant distributions, in addition to the Poisson ($k = 0$) distribution of trap energies. We provide the details in Section S7 and discuss the key results here. The Poisson ($k = 2$) and the hyperbolic secant distributions enhance the division in the coverages of the methanol molecule at 80 K, while reducing the division in the other coverages. Only the normal distribution predicts a significant reduction of the division in all of the coverages. On the one hand, the normal and the hyperbolic secant distributions evoke the deep trap states in the middle of the band gap, rather than the shallow trap states at the band edge. As discussed in Methods, it is dubious whether the mid-gap states can participate in the photochemistry. Thus, we continue to prefer the Poisson distribution. On the other hand, the division appears to be quite insensitive to the type of static disorder, as long as the distribution of trap energies has a long tail. Hence, the emergence of the two groups might play a significant role in a variety of photocatalytic processes on TiO_2.

Conclusion

We have described a novel method to simulate the chemical kinetics of methanol oxidation on TiO_2. Combining the intuition of MFSS with PA, HHPA can describe the effects of static disorder and dynamic correlation at the same time. Furthermore, pre-averaging over the static disorder in one site of each pair makes HHPA efficient enough to simulate systems of several species and calibrate rate constants.

The simulated kinetics indicate that the dominant hole scavengers are temperature-dependent – the methoxy anion at 80 K and the methanol molecule at 180 K. Even though the thermally activated cleavage of the OH bond is orders of magnitude faster, the methoxy

anion tends to revert to the methanol molecule before it traps a hole. Thus, the hole-activated cleavage of the OH bond determines the overall kinetics at 180 K. Static disorder in the hole transfer steps appears to explain the stretched exponentials in the observed kinetics. Remarkably, two groups of Ti_{5c} sites emerge with innate and disparate activities, even though no such division exists in the underlying rate constants. Since the division appears to be quite insensitive to the type of static disorder, the emergence of two groups might play a significant role in a variety of photocatalytic processes on TiO_2.

Based on these results, we propose a number of directions that require attention in the future. Concerning TiO_2 and methanol oxidation in particular, it would be of both practical and theoretical interest to determine whether the high-activiy sites and the low-activity sites retain their individual properties when the surface is cleaned and a new layer of adsorbates is deposited. Furthermore, there are few systematic studies of the chemical kinetics at ranges of temperatures, coverages, and defect densities that would help identify the mechanistic regimes that might exist. Concerning chemical kinetics in general, it might be of interest to identify and classify systems where a combination of static disorder and dynamic correlations has non-trivial effects on chemical kinetics.

Acknowledgement

This study has been supported by the ACS Petroleum Research Fund (60503-ND6).

Supporting Information Available

Demonstration of HMF and HHPA on a number of simple model systems; cross-examination of calibrated parameters in the MF and the PA methods; simulated kinetics in the modified model; sensitivity analysis of the calibrated parameters in the original model and the modified model; construction and outcomes of the compact model; extended discussion on the origin of the bimodal distributions in the coverages and the rates; distributions of the coverages

and the rates in the original, modified, and compact models; and normal, Poisson ($k = 2$), and hyperbolic secant distributions of trap energies.

References

(1) Emonts, B.; Bgild Hansen, J.; Lgsgaard Jrgensen, S.; Hhlein, B.; Peters, R. Compact methanol reformer test for fuel-cell powered light-duty vehicles. *J. Power Sources* **1998**, *71*, 288–293.

(2) Wiese, W.; Emonts, B.; Peters, R. Methanol steam reforming in a fuel cell drive system. *J. Power Sources* **1999**, *84*, 187–193.

(3) Peters, R.; Dsterwald, H.; Hhlein, B. Investigation of a methanol reformer concept considering the particular impact of dynamics and long-term stability for use in a fuel-cell-powered passenger car. *J. Power Sources* **2000**, *86*, 507–514.

(4) Olah, G. A. Beyond Oil and Gas: The Methanol Economy. *Angew. Chem. Int. Edit.* **2005**, *44*, 2636–2639.

(5) Kawai, T.; Sakata, T. Photocatalytic hydrogen production from liquid methanol and water. *J. Chem. Soc. Chem. Comm.* **1980**, 694–695.

(6) Kawai, M.; Naito, S.; Tamaru, K.; Kawai, T. The mechanism of photocatalytic hydrogen production from gaseous methanol and water: IR spectroscopic approach. *Chem. Phys. Lett.* **1983**, *98*, 377–380.

(7) Dickinson, A.; James, D.; Perkins, N.; Cassidy, T.; Bowker, M. The photocatalytic reforming of methanol. *J. Mol. Catal. A-Chem.* **1999**, *146*, 211–221.

(8) Zhou, C. et al. Site-specific photocatalytic splitting of methanol on TiO_2(110). *Chem. Sci.* **2010**, *1*, 575–580.

(9) Zhou, C.; Ma, Z.; Ren, Z.; Mao, X.; Dai, D.; Yang, X. Effect of defects on photocatalytic dissociation of methanol on TiO_2(110). *Chem. Sci.* **2011**, *2*, 1980–1983.

(10) Feng, H.; Tan, S.; Tang, H.; Zheng, Q.; Shi, Y.; Cui, X.; Shao, X.; Zhao, A.; Zhao, J.; Wang, B. Temperature- and Coverage-Dependent Kinetics of Photocatalytic Reaction of Methanol on TiO_2 (110)-(1 1) Surface. *J. Phys. Chem. C* **2016**, *120*, 5503–5514.

(11) Tan, S.; Feng, H.; Ji, Y.; Zheng, Q.; Shi, Y.; Zhao, J.; Zhao, A.; Yang, J.; Luo, Y.; Wang, B.; Hou, J. G. Visualizing Elementary Reactions of Methanol by Electrons and Holes on TiO_2(110) Surface. *J. Phys. Chem. C* **2018**, *122*, 28805–28814.

(12) Guo, Q.; Xu, C.; Ren, Z.; Yang, W.; Ma, Z.; Dai, D.; Fan, H.; Minton, T. K.; Yang, X. Stepwise Photocatalytic Dissociation of Methanol and Water on TiO_2(110). *J. Am. Chem. Soc.* **2012**, *134*, 13366–13373.

(13) Migani, A.; Blancafort, L. Excitonic Interfacial Proton-Coupled Electron Transfer Mechanism in the Photocatalytic Oxidation of Methanol to Formaldehyde on TiO_2(110). *J. Am. Chem. Soc.* **2016**, *138*, 16165–16173.

(14) Zhang, J.; Peng, C.; Wang, H.; Hu, P. Identifying the Role of Photogenerated Holes in Photocatalytic Methanol Dissociation on Rutile TiO_2(110). *ACS Catal.* **2017**, *7*, 2374–2380.

(15) Jin, F.; Zhang, X.; Wei, M.; Chen, T.; Ma, H.; Ma, Y. Critical role of the defect state in the photo-oxidation of methanol on TiO_2(110). *J. Mater. Chem. A* **2020**, *8*, 20082–20090.

(16) Micic, O.; Zhang, Y.; Cromack, K. R.; Trifunac, A.; Thurnauer, M. Photoinduced hole transfer from titanium dioxide to methanol molecules in aqueous solution studied by electron paramagnetic resonance. *J. Phys. Chem.* **1993**, *97*, 13284–13288.

(17) Yamakata, A.; Ishibashi, T.-a.; Onishi, H. Electron- and Hole-Capture Reactions on Pt/TiO_2 Photocatalyst Exposed to Methanol Vapor Studied with Time-Resolved Infrared Absorption Spectroscopy. *J. Phys. Chem. B* **2002**, *106*, 9122–9125.

(18) Tamaki, Y.; Furube, A.; Murai, M.; Hara, K.; Katoh, R.; Tachiya, M. Direct Observation of Reactive Trapped Holes in TiO_2 Undergoing Photocatalytic Oxidation of Adsorbed Alcohols: Evaluation of the Reaction Rates and Yields. *J. Am. Chem. Soc.* **2006**, *128*, 416–417.

(19) Wang, T.; Hao, Q.; Wang, Z.; Mao, X.; Ma, Z.; Ren, Z.; Dai, D.; Zhou, C.; Yang, X. Deuterium Kinetic Isotope Effect in the Photocatalyzed Dissociation of Methanol on TiO2(110). *J. Phys. Chem. C* **2018**, *122*, 26512–26518.

(20) Kopelman, R. Fractal Reaction Kinetics. *Science* **1988**, *241*, 1620–1626.

(21) Moiny, F.; Dumont, M.; Dagonnier, R. Fractal kinetics and surface reactions. *J. Chem. Phys.* **1998**, *108*, 4572–4581.

(22) Mao, X.; Wei, D.; Wang, Z.; Jin, X.; Hao, Q.; Ren, Z.; Dai, D.; Ma, Z.; Zhou, C.; Yang, X. Recombination of Formaldehyde and Hydrogen Atoms on $TiO_2(110)$. *J. Phys. Chem. C* **2015**, *119*, 1170–1174.

(23) Thompson, T. L.; Yates, J. T. Monitoring Hole Trapping in Photoexcited $TiO_2(110)$ Using a Surface Photoreaction. *J. Phys. Chem. B* **2005**, *109*, 18230–18236.

(24) Thompson, T. L.; Yates, J. T. Control of a Surface Photochemical Process by Fractal Electron Transport Across the Surface: O2 Photodesorption from $TiO_2(110)$. *J. Phys. Chem. B* **2006**, *110*, 7431–7435.

(25) Pang, C. L.; Lindsay, R.; Thornton, G. Chemical reactions on rutile $TiO_2(110)$. *Chem. Soc. Rev.* **2008**, *37*, 2328–2353.

(26) Wendt, S.; Sprunger, P. T.; Lira, E.; Madsen, G. K. H.; Li, Z.; Hansen, J. Ø.; Matthiesen, J.; Blekinge-Rasmussen, A.; Lægsgaard, E.; Hammer, B.; Besenbacher, F. The Role of Interstitial Sites in the Ti_{3d} Defect State in the Band Gap of Titania. *Science* **2008**, *320*, 1755–1759.

(27) Deskins, N. A.; Rousseau, R.; Dupuis, M. Defining the Role of Excess Electrons in the Surface Chemistry of TiO_2. *J. Phys. Chem. C* **2010**, *114*, 5891–5897.

(28) Haubrich, J.; Kaxiras, E.; Friend, C. M. The Role of Surface and Subsurface Point Defects for Chemical Model Studies on TiO_2: A First-Principles Theoretical Study of Formaldehyde Bonding on Rutile TiO_2(110). *Chem. Eur. J.* **2011**, *17*, 4496–4506.

(29) Zhang, Z.; Tang, M.; Wang, Z.-T.; Ke, Z.; Xia, Y.; Park, K. T.; Lyubinetsky, I.; Dohnálek, Z.; Ge, Q. Imaging of Formaldehyde Adsorption and Diffusion on TiO_2(110). *Top. Catal.* **2015**, *58*, 103–113.

(30) Geva, N.; Vaissier, V.; Shepherd, J.; Van Voorhis, T. Mean field treatment of heterogeneous steady state kinetics. *Chem. Phys. Lett.* **2017**, *685*, 185–190.

(31) McIsaac, A. R.; Vaissier Welborn, V.; Einzinger, M.; Geva, N.; Weir, H.; Baldo, M. A.; Van Voorhis, T. Investigation of External Quantum Efficiency Roll-Off in OLEDs Using the Mean-Field Steady-State Kinetic Model. *J. Phys. Chem. C* **2020**, *124*, 14424–14431.

(32) Dickman, R. Kinetic phase transitions in a surface-reaction model: Mean-field theory. *Phys. Rev. A* **1986**, *34*, 4246–4250.

(33) Matsuda, H. In *Animal Societies: Theories and Facts*; Ito, Y., Brown, J. P., Kikkawa, J., Eds.; Japan Scientific Societies Press: Tokyo, 1987; pp 67–80.

(34) Matsuda, H.; Ogita, N.; Sasaki, A.; Satō, K. Statistical Mechanics of Population: The Lattice Lotka-Volterra Model. *Prog. Theor. Phys.* **1992**, *88*, 1035–1049.

(35) Keeling, M. J.; Rand, D. A.; Morris, A. J. Correlation models for childhood epidemics. *Proc. R. Soc. Lond. B* **1997**, *264*, 1149–1156.

(36) Gillespie, D. T. A General Method for Numerically Simulating the Stochastic Time Evolution of Coupled Chemical Reactions. *J. Comput. Phys.* **1976**, *22*, 403–434.

(37) Voter, A. F. In *Radiation Effects in Solids*; Sickafus, K. E., Kotomin, E. A., Uberuaga, B. P., Eds.; Springer Netherlands: Dordrecht, 2007; pp 1–23.

(38) Chatterjee, A.; Vlachos, D. G. An overview of spatial microscopic and accelerated kinetic Monte Carlo methods. *J. Comput. Aided Mater. Des.* **2007**, *14*, 253–308.

(39) Whittle, P. On the Use of the Normal Approximation in the Treatment of Stochastic Processes. *J. R. Stat. Soc. B* **1957**, *19*, 268–281.

(40) Gómez-Uribe, C. A.; Verghese, G. C. Mass fluctuation kinetics: Capturing stochastic effects in systems of chemical reactions through coupled mean-variance computations. *J. Chem. Phys.* **2007**, *126*, 024109.

(41) Keeling, M. J. Multiplicative Moments and Measures of Persistence in Ecology. *J. Theor. Biol.* **2000**, *205*, 269–281.

(42) Nåsell, I. An extension of the moment closure method. *Theor. Popul. Biol.* **2003**, *64*, 233–239.

(43) Schnoerr, D.; Sanguinetti, G.; Grima, R. Comparison of different moment-closure approximations for stochastic chemical kinetics. *J. Chem. Phys.* **2015**, *143*, 185101.

(44) Pugliese, E.; Castellano, C. Heterogeneous pair approximation for voter models on networks. *EPL* **2009**, *88*, 58004.

(45) Mata, A. S.; Ferreira, R. S.; Ferreira, S. C. Heterogeneous pair-approximation for the contact process on complex networks. *New J. Physics* **2014**, *16*, 053006.

(46) Kermack, W. O.; McKendrick, A. G.; Walker, G. T. A contribution to the mathematical theory of epidemics. *P. R. Soc. Lond. A-Conta.* **1927**, *115*, 700–721.

(47) Holley, R. A.; Liggett, T. M. Ergodic Theorems for Weakly Interacting Infinite Systems and the Voter Model. *Ann. Probab.* **1975**, *3*, 643 – 663.

(48) Diebold, U. The surface science of titanium dioxide. *Surf. Sci. Rep.* **2003**, *48*, 53–229.

(49) Bates, S. P.; Gillan, M. J.; Kresse, G. Adsorption of Methanol on TiO_2(110): A First-Principles Investigation. *J. Phys. Chem. B* **1998**, *102*, 2017–2026.

(50) A. Henderson, M.; Otero-Tapia, S.; E. Castro, M. The chemistry of methanol on the TiO_2(110) surface: the influence of vacancies and coadsorbed species. *Faraday Discuss.* **1999**, *114*, 313–329.

(51) de Armas, R. S.; Oviedo, J.; San Miguel, M. A.; Sanz, J. F. Methanol Adsorption and Dissociation on TiO_2(110) from First Principles Calculations. *J. Phys. Chem. C* **2007**, *111*, 10023–10028.

(52) Zhao, J.; Yang, J.; Petek, H. Theoretical study of the molecular and electronic structure of methanol on a TiO_2(110) surface. *Phys. Rev. B* **2009**, *80*, 235416.

(53) Yuan, Q.; Wu, Z.; Jin, Y.; Xu, L.; Xiong, F.; Ma, Y.; Huang, W. Photocatalytic Cross-Coupling of Methanol and Formaldehyde on a Rutile TiO2(110) Surface. *J. Am. Chem. Soc.* **2013**, *135*, 5212–5219.

(54) Shen, M.; Henderson, M. A. Identification of the Active Species in Photochemical Hole Scavenging Reactions of Methanol on TiO_2. *J. Phys. Chem. Lett.* **2011**, *2*, 2707–2710.

(55) Nelson, J. Continuous-time random-walk model of electron transport in nanocrystalline TiO_2 electrodes. *Phys. Rev. B* **1999**, *59*, 15374–15380.

(56) Pascual, J.; Camassel, J.; Mathieu, H. Fine structure in the intrinsic absorption edge of TiO_2. *Phys. Rev. B* **1978**, *18*, 5606–5614.

(57) Amtout, A.; Leonelli, R. Optical properties of rutile near its fundamental band gap. *Phys. Rev. B* **1995**, *51*, 6842–6851.

(58) Urbach, F. The Long-Wavelength Edge of Photographic Sensitivity and of the Electronic Absorption of Solids. *Phys. Rev.* **1953**, *92*, 1324–1324.

Graphical TOC Entry